Acta Pharmaceutica Sinica B 2024;14(1):207−222

Chinese Pharmaceutical Association
Institute of Materia Medica, Chinese Academy of Medical Sciences

Acta Pharmaceutica Sinica B

www.elsevier.com/locate/apsb
www.sciencedirect.com

ORIGINAL ARTICLE

# A novel TNKS/USP25 inhibitor blocks the Wnt pathway to overcome multi-drug resistance in TNKS-overexpressing colorectal cancer

**Hongrui Zhu[a,†], Yamin Gao[a,†], Liyun Liu[a,†], Mengyu Tao[b], Xiao Lin[c], Yijia Cheng[a], Yaoyao Shen[a], Haitao Xue[a], Li Guan[a], Huimin Zhao[a], Li Liu[d], Shuping Wang[a], Fan Yang[a], Yongjun Zhou[a], Hongze Liao[a], Fan Sun[a,*], Houwen Lin[a,e,*]**

[a]*Research Center for Marine Drugs, Department of Pharmacy, Ren Ji Hospital, Shanghai Jiao Tong University School of Medicine, Shanghai 200127, China*
[b]*Department of Oncology, Shanghai General Hospital, Shanghai Jiao Tong University School of Medicine, Shanghai 200080, China*
[c]*Institute of Marine Drugs, Guangxi University of Chinese Medicine, Nanning 530200, China*
[d]*State Key Laboratory of New Drug and Pharmaceutical Process, Shanghai Professional and Technical Ser-vice Center for Biological Material Drug-ability Evaluation, Shanghai Institute of Pharmaceutical Industry, China State Institute of Pharmaceutical Industry, Shanghai 200437, China*
[e]*Institute of Marine Biomedicine, Shenzhen Polytechnic, Shenzhen 518055, China*

Received 16 July 2023; received in revised form 29 August 2023; accepted 11 October 2023

**KEY WORDS**

Colorectal cancer;
TNKS−USP25 interaction;
Multi-drug resistance;
TNKS overexpression;
Wnt pathway;
Apoptosis;
Neoantimycin analog

**Abstract** Modulating Tankyrases (TNKS), interactions with USP25 to promote TNKS degradation, rather than inhibiting their enzymatic activities, is emerging as an alternative/specific approach to inhibit the Wnt/$\beta$-catenin pathway. Here, we identified UAT-B, a novel neoantimycin analog isolated from *Streptomyces conglobatus*, as a small-molecule inhibitor of TNKS−USP25 protein−protein interaction (PPI) to overcome multi-drug resistance in colorectal cancer (CRC). The disruption of TNKS−USP25 complex formation by UAT-B led to a significant decrease in TNKS levels, triggering cell apoptosis through modulation of the Wnt/$\beta$-catenin pathway. Importantly, UAT-B successfully inhibited the CRC cells growth that harbored high TNKS levels, as demonstrated in various *in vitro* and *in vivo* studies utilizing cell line-based and patient-derived xenografts, as well as $APC^{min/+}$ spontaneous CRC models. Collectively, these

*Corresponding authors.
E-mail addresses: sunfan2017@163.com (Fan Sun), hwlin@sjtu.edu.cn (Houwen Lin).
†These authors made equal contributions to this work.
Peer review under the responsibility of Chinese Pharmaceutical Association and Institute of Materia Medica, Chinese Academy of Medical Sciences.

https://doi.org/10.1016/j.apsb.2023.10.013

findings suggest that targeting the TNKS−USP25 PPI using a small-molecule inhibitor represents a compelling therapeutic strategy for CRC treatment, and UAT-B emerges as a promising candidate for further preclinical and clinical investigations.



## 1. Introduction

Colorectal cancer (CRC) is the third most commonly diagnosed cancer and the fourth leading cause of cancer-related death worldwide[1]. Multi-drug resistance (MDR), which develops when cancer cells become resistant to multiple antineoplastic drugs having different structures and mechanisms during the course of tumor therapy, is a major challenge in CRC treatment[2]. The discovery of novel drugs/targets and a deeper understanding of resistance mechanisms can lead to the development of additional therapeutic strategies to overcome resistance. The Cancer Genome Atlas (TCGA) revealed that 93% of CRCs have hyperactivation of the Wnt pathway[3], in approximately 90% of cases due to mutations in the *adenomatosis polyposis coli* (*APC* ) gene (a major suppressor of the Wnt pathway) or *CTNNB1* (which encodes $\beta$-catenin)[4]. Given the critical function of the Wnt pathway in managing malignant progression, it has been associated with oncogenic incidents and implicated in the modulation of immune responses, tumor survival, and metabolic changes, all of which contribute to tumorigenesis[5]. Further, the involvement of the Wnt pathway in the development of multi-drug resistance poses significant challenges by diminishing the effectiveness of therapeutic agents[6]. Hence, the pharmacological intervention of the Wnt pathway could potentially serve as a promising avenue for developing antitumor therapies, especially for the treatment of MDR cancers.

Tankyrases (TNKS), distinct members of the poly (ADP-ribose) polymerase (PARP) family[7], serve as critical regulators of Wnt signaling transduction. They enhance Wnt pathway activity through PARylation and subsequent proteolysis of Axin (also known as Axin 1)[8,9], a factor whose concentration limits the efficiency of the $\beta$-catenin destruction complex[10]. Thus, pharmacological inhibition of TNKS leads to an accumulation of Axin1, causing concomitant degradation of $\beta$-catenin and suppression of the proliferation of various *APC*-mutated CRC cells[11,12]. Moreover, analysis of long-term outcomes revealed that high expression of TNKS1 (also known as TNKS) was significantly correlated with poorer overall survival in both lung adenocarcinoma and lung squamous cell carcinoma patients[13]. Given these findings, TNKS has emerged as a potential new therapeutic target for treating cancers with dysregulated Wnt activity. TNKS influence the Wnt pathway in cancer cells through both catalysis-dependent and catalysis-independent functions[14]. However, currently reported TNKS inhibitors (TNKSi) not only effectively inhibit TNKS catalytic activity, but also increase its protein expression level[15]. Therefore, the efficacy of catalytic TNKSi may be compromised in cancers exhibiting high levels of TNKS.

The ubiquitin system represents a crucial protein regulation mechanism, controlling a diverse array of cellular processes[16]. Recent findings suggest that ubiquitin-specific protease 25 (USP25), a deubiquitinating enzyme (DUB), stabilizes TNKS by directly binding its C-terminus to the ankyrin repeats (ARCs) in TNKS[17]. Notably, these ARCs are absent in other members of the PARP family, thus presenting a unique opportunity for selectively targeting TNKS[18]. Thus, disrupting this interaction to promote the degradation rather than inhibiting TNKS enzymatic activity may provide a novel opportunity for effective Wnt-dependent cancer therapy. However, the role of this mechanism in CRC remains to be elucidated.

Antimycin-type depsipeptides are a family of natural products that have attracted considerable interest owing to their notable anticancer activities[19]. Unantimycin B (UAT-B) (Fig. 1A), a unique neoantimycin analog extracted from *Streptomyces conglobatus*, is a novel compound our group has identified. We previously reported that UAT-B exhibited considerable anticancer activity, particularly against the CRC cell line SW620. Importantly, unlike the severe toxicities typically associated with antimycin-type natural products, UAT-B showed no significant toxicity toward non-malignant cells[20]. Nevertheless, the precise anticancer activity and mechanisms of UAT-B have not been fully characterized.

In this study, we report that UAT-B displayed potent antitumor efficacy against CRC, particularly in cells with high TNKS levels activating the Wnt pathway. This was evidenced through multiple cell-based assays and a variety of *in vivo* models, including cell line-derived and patient-derived xenograft models, as well as the genetically engineered $APC^{min/+}$ model of spontaneous CRC. Remarkably, UAT-B's anti-CRC effects were also evident in TNKSi-resistant and chemotherapeutic drug-resistant CRC cells. Mechanistically, UAT-B disrupts the TNKS−USP25 interaction, promoting TNKS degradation and subsequently stabilizing Axin 1, thereby inhibiting the Wnt pathway, which was first identified and demonstrated in CRC. In summary, our study provides evidence that inhibition of the TNKS−USP25 interaction is a novel therapeutic approach to counteract the MDR of CRC, and highlights UAT-B as a promising lead compound for enhancing our understanding of TNKS as a target in CRC therapy.

## 2. Materials and methods

### 2.1. Reagents and materials

MG-132 was purchased from Sigma−Aldrich (SML1135, Missouri, USA). PageRuler™ Prestained Protein Ladder (10−180 kDa, 26616), RIPA Lysis and Extraction Buffer (89900) and Pierce IP Lysis Buffer (87787) were purchased from Thermo Fisher Scientific (Eugene, USA). Anti-mouse IgG, and HRP-linked antibody (1:3000, 7076) and anti-rabbit IgG, HRP-linked antibody (1:3000, 7074) were purchased from Cell Signaling Technology (MA, USA).

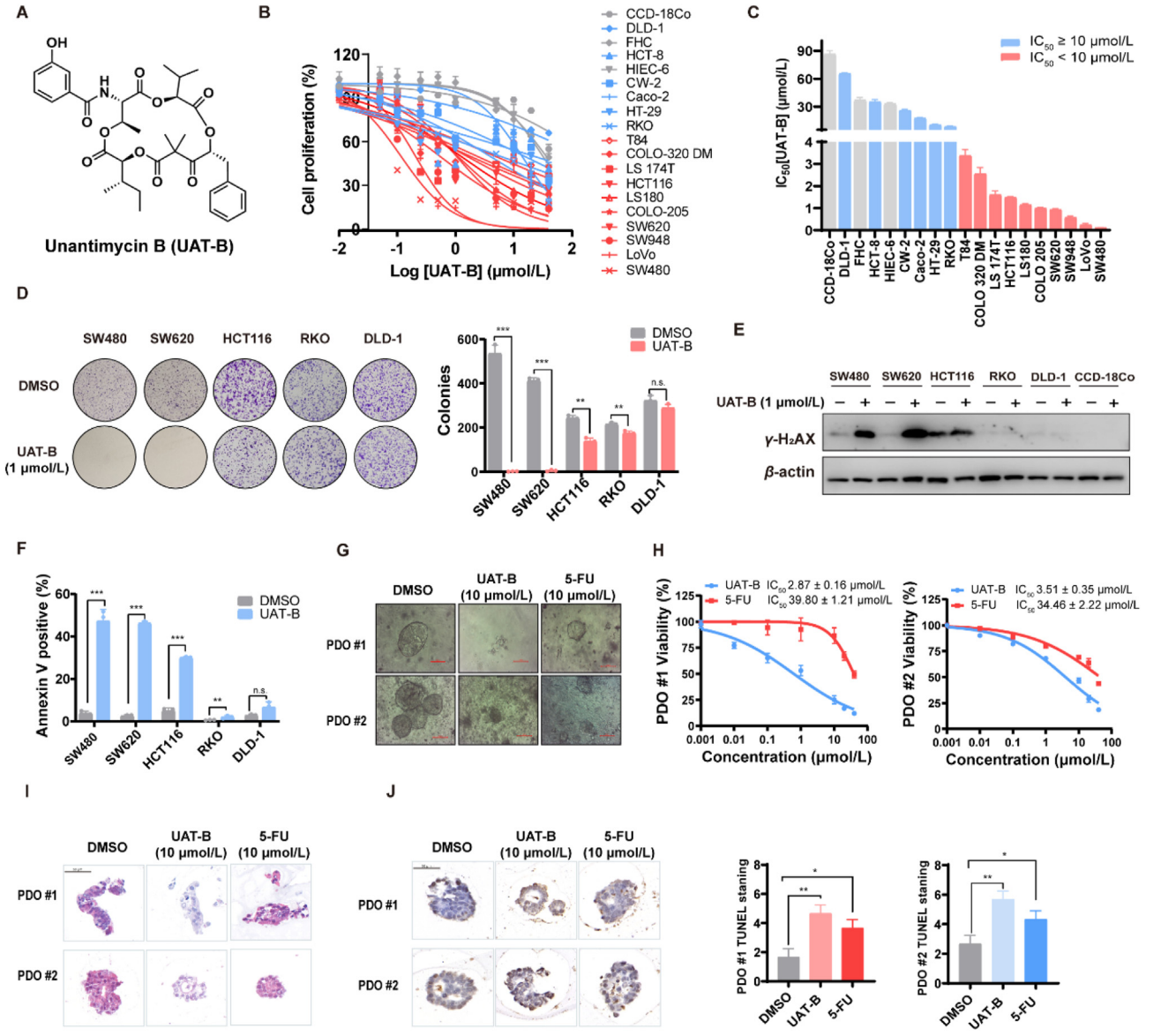


**Figure 1** UAT-B selectively induces apoptosis in various CRC cell lines and PDOs. (A) Chemical structure of UAT-B. (B) Dose responses of the proliferation of various CRC cell lines and non-malignant cells exposed to UAT-B for 48 h were determined by CCK-8 assay. Grey line, non-malignant cells with $IC_{50}$ values; blue lines, CRC cell lines with $IC_{50}$ values greater than 10 μmol/L; red lines, less than 10 μmol/L. (C) The $IC_{50}$ values of UAT-B in various CRC cell lines and non-malignant colorectal cells following 48 h treatment. (D)−(F) Effects of UAT-B inhibition in SW480, SW620, HCT116, RKO and DLD-1 cells assayed by colony formation analysis (D), Western blot analysis for γ-$H_2AX$ (E) and flow cytometry analysis for apoptosis (F). (G) The representative photomicrographs of two CRC PDOs (PDO #1−2) treated with DMSO or with UAT-B or with 5-FU (20× magnification). Scale bars, 100 μm. (H) PDOs were treated with the indicated concentrations of UAT-B or 5-FU for 72 h, and cell viability was measured by CellTiter-Lumi™. (I) H&E staining of PDOs treated with UAT-B or 5-FU. Scale bars, 50 μm. (J) Representative images of TUNEL staining and quantification of TUNEL H-Score. Scale bars, 50 μm. The data represent the mean ± SD from three independent experiments. *$P < 0.05$, **$P < 0.01$, ***$P < 0.001$; n.s., statistically not significant.

### 2.2. *Patient-derived organoids*

Tumor samples were obtained from CRC patients at Renji Hospital for short-term organoid generation and subsequent experiments. Written informed consent was obtained from all subjects, and the study was approved by the Ethics Committee of Shanghai Jiao tong University School of Medicine, Renji Hospital. Organoids were suspended in Matrigel (200−500/μL) and seeded in a 96-well plate at 20 μL per well. When the Matrigel solidified, 80 μL of complete culture medium was added to each well. The drugs were added 72 h after embedding. Cell viability was assayed using CellTiter-Lumi™ (Beyotime, Shanghai, China). $IC_{50}$ values were calculated using the GraphPad Prism 9.0.

### 2.3. *Colony formation assay*

Cells were seeded in six-well plates (1500 cells per well), exposed to DMSO, UAT-B, or G007-LK treatments, and cultured in a

complete medium for approximately two weeks. The cells were then fixed with 4% paraformaldehyde for 15 min and stained with 0.01% crystal violet (Beyotime, Shanghai, China).

### 2.4. Apoptosis assay by Annexin V-PI staining

Apoptosis analysis was performed using the Annexin V-FITC/PI Apoptosis Detection Kit (Dojindo, Kumamoto, Japan). The cells were seeded in 24-well plates at 50% confluence and treated with DMSO or UAT-B for 48 h. Then, the cells were harvested, washed twice with ice-cold PBS, and resuspended in 1 × binding buffer containing 5 μL Annexin V-FITC and 5 μL PI for 15 min at room temperature (RT) in the dark. After labeling, 400 μL of 1 × binding buffer was added into each sample before performing flow cytometry analysis (Thermo Fisher Scientific, Eugene, USA).

### 2.5. TOP/FOP flash luciferase reporter assay

The cells were seeded in 24-well plates and cultured for 24 h. Cells were transiently co-transfected 0.5 μg TCF/LEF reporter plasmid or the mutant TCF/LEF reporter plasmid and 0.05 μg Renilla luciferase plasmid for normalization, using X-tremeGENE HP DNA Transfection Reagent (Roche, Basel, Germany). After transfection for 24 h, the cells were treated with UAT-B, lysed in passive lysis buffer, and harvested for luciferase activity assay (Promega, Fitchburg, USA).

### 2.6. Immunofluorescence (IF)

The cells were fixed with 4% paraformaldehyde (30 min), permeabilized using 0.3% Triton X-100 (15 min) with an additional 1 h for blocking in 5% BSA. Cells were sequentially incubated with indicated primary antibodies overnight at 4 °C. Then, the cells were incubated with a secondary antibody at RT for 1 h. The nuclei were counterstained with DAPI for 5 min. Finally, fluorescence images were captured and merged using a laser confocal microscope (Leica SP8, Weztlar, Germany).

### 2.7. Immunoprecipitation

Cells were incubated with lysis buffer containing protease inhibitors and PMSF for 30 min at 4 °C. After quantification, appropriate cell lysates were incubated with specific antibodies, rotating overnight at 4 °C. 20 μL of Pierce™ Protein A/G Magnetic Beads (Thermo, #88802) was then added to each sample and rotated for 2 h at 4 °C. The beads were washed four times with lysis buffer, and the immune complexes were eluted at 95 °C for 5 min with 1 × loading buffer. The immunoprecipitated complexes were then separated by SDS/PAGE and subjected to Western blot analysis.

### 2.8. Western blot analysis

The cells were resuspended in RIPA lysis buffer and incubated on ice for 30 min. After centrifugation at 12,000 rpm for 10 min at 4 °C, the supernatant fractions were harvested. Protein concentration was detected using the BCA Quantification kit (Beyotime Biotechnology, Shanghai, China, Cat#P0011). Next, the protein extract was resolved by SDS/PAGE and transferred to PVDF (Millipore, MA, USA) membranes. Membranes were blocked for 1 h at RT followed by appropriate primary antibodies overnight at 4 °C and subsequently incubated with secondary antibodies conjugated with horseradish peroxidase for 2 h at RT. Specific protein bands in the membrane were visualized using an enhanced chemiluminescence (ECL) reagent (NCM Biotech, Suzhou, China) and Amersham Imager 600 (GE Healthcare, Fairfield, USA). The dilution of antibody in this study are listed in Supporting Information Table S6.

### 2.9. Cellular thermal shift assay (CETSA)

Cells were seeded in 10-cm cell culture dishes and grown to ~90% confluence. Subsequently, the cells were treated with DMSO or UAT-B (1 μmol/L) for 8 h. After trypsination and PBS washing, cells were resuspended in 700 μL PBS containing freshly added protease inhibitors and equally divided into seven tubes. Cells in each tube were heated at the indicated temperature endpoints (38−48 °C) for 3 min in a PCR thermocycler and at RT for another 3 min. Heated cells were lysed by three cycles of freezing in liquid nitrogen (1 min) and thawing in water at RT (1 min). Each cell lysate was centrifuged (15,000 rpm for 20 min at 4 °C). The soluble fractions were isolated for Western blot analysis.

### 2.10. Proximity ligation assay (PLA)

Proximity Ligation Assay (PLA) was performed by the Duolink® In situ Red Starter Kit Mouse/Rabbit (Sigma−Aldrich). Briefly, the cells were fixed with 4% paraformaldehyde for 15 min, permeabilized with 0.3% Triton X-100 (15 min) and an additional 1 h for blocking in 5% BSA. After blocking, the cells were incubated with pre-diluted primary antibodies overnight at 4 °C. The subsequent step was incubating the pre-diluted anti-rabbit plus and anti-mouse minus probes at 37 °C for 1 h. Then, samples were incubated with 1 × ligation buffer containing ligase for 30 min at 37 °C, then incubated with 1 × amplification solution containing the polymerase for 100 min at 37 °C. Finally, coverslips were mounted on the slide with Duolink® In situ Mounting Medium with DAPI. After approximately 15 min, slides were analyzed by confocal microscopy (Leica SP8, Weztlar, Germany) using a 63× objective.

### 2.11. CDX and PDX mouse models

All experimental procedures using animals were in accordance with the guidelines provided by the Animal Ethics Committee of Shanghai Model Organisms Center (Shanghai, China). Six-to eight-week-old BALB/c nude mice (Shanghai Jihui Laboratory Animal Care Co., Ltd., China) were randomly divided into five or six groups as follows: Vehicle ($n = 6$); UAT-B 0.5 mg/kg ($n = 6$); UAT-B 1 mg/kg ($n = 6$); G007-LK 20 mg/kg ($n = 6$); 5-FU 20 mg/kg ($n = 6$) (SW480 and RKO CDX mouse models) or Vehicle ($n = 6$); 5-FU 20 mg/kg ($n = 6$); UAT-B 1 mg/kg ($n = 6$); G007-LK 20 mg/kg ($n = 6$); 5-FU 10 mg/kg + UAT-B 0.5 mg/kg ($n = 6$); 5-FU 10 mg/kg + G007-LK 10 mg/kg ($n = 6$) (HCT-8/5-FU CDX mouse models). CRC Cells ($1 \times 10^7$ cells) suspended in 100 μL of PBS were subcutaneously injected into the flank of BALB/c nude mice. The mice received an intraperitoneal injection of the vehicle or designated doses every day. Tumor volumes were measured using calipers and calculated using Eq. (1):

$$\text{Tumor volume} = (L \times W^2)/2 \quad (1)$$

where $L$ and $W$ refer to the tumor diameter along the longitudinal and transverse axes. After treatment or meeting the humane

endpoint criteria, the mice were sacrificed. The tumors were dissected, imaged, and weighed. Tumor tissues were collected, fixed in 10% neutral buffered formalin, or snap frozen in liquid $N_2$ and stored at −80 °C for subsequent analyses. PDX studies were conducted at Crown Bioscience Inc. (Taicang, China; San Diego, CA, USA) under the instruction and supervision of Tingting Zhang's laboratory.

### 2.12. *APC$^{min/+}$ mouse model*

C57BL/6J-*APC$^{min/+}$* mice were obtained from Jackson Laboratory. Eight-week-old male mice of the same parental generation were divided into two groups that received 1 mg/kg UAT-B or vehicle via intraperitoneal injection every other day. The mice were sacrificed and tumors of longitudinal dissection of the small intestine and colon were imaged. Tumor numbers were calculated. Then, the small intestines and colons were sectioned and stained with immunohistochemistry. The survival time of mice after UAT-B treatment was recorded.

### 2.13. *Statistical analysis*

Significance was evaluated with ANOVA or two-tailed Student's *t*-tests unless otherwise indicated in the figure legends. *P* values less than 0.05 were considered significant. The graphs and error bars show the mean ± SD of three independent biological experiments unless stated otherwise. All statistical analyses were performed using GraphPad Prism V9.

## 3. Results

### 3.1. *UAT-B selectively induces apoptotic effects across diverse CRC cells*

Our group previously reported that UAT-B (Fig. 1A) exhibited selective anticancer activity, especially against CRC cells[20]. In this study, we further explored the effects of UAT-B on the viability of various cultured CRC cells and non-malignant cells. Our findings revealed UAT-B significantly inhibited CRC cell activity in a dose-dependent manner (Fig. 1B), with half-maximum inhibitory concentration ($IC_{50}$) values ranging from 0.11 to 65.46 μmol/L (Fig. 1C and Supporting Information Table S1). This implies the potential of UAT-B for broad-spectrum targeting of CRC cells. Importantly, when compared to the CRC cell line SW480, the $IC_{50}$ values of UAT-B against non-malignant colorectal cells (CCD-18Co, FHC, and HIEC-6) were approximately 880, 370, and 330 times greater, respectively, highlighting lower cytotoxicity of UAT-B towards normal cells (Table S1). *In vitro* colony formation assay results indicated that the clonal survival of SW480, SW620, and HCT116 cells was markedly inhibited by 1 μmol/L UAT-B (Fig. 1D). However, this was not observed in RKO and DLD-1 cells. We noted that γ-$H_2AX$ levels were elevated in SW480, SW620, and HCT116 cells, but not in RKO, DLD-1, and CCD-18Co cells following 48 h of UAT-B treatment (Fig. 1E). Similar patterns were seen in the apoptosis analysis of these CRC cell lines in response to UAT-B (Fig. 1F). Patient-derived organoids (PDOs) have the advantage of maintaining the genetic stability of the original tumor over a longer period compared to traditional adherent monolayer cultures. This allows them to more accurately model the patient's tumor and its microenvironment, making them a valuable tool for preclinical therapeutic testing and development[21]. We assessed the clinical potential of UAT-B in two independent CRC tumor-derived organoids (PDO#1, #2) using the CellTiter-Lumi™ assay. Compared to 5-fluorouracil (5-FU), UAT-B significantly inhibited the growth of both CRC PDOs (Fig. 1G and H). Hematoxylin and eosin (H&E) and TUNEL staining corroborated that UAT-B treatment induced substantial tumor necrosis (Fig. 1I) and apoptosis (Fig. 1J) in both PDOs. Collectively, these findings affirm that UAT-B exhibits selective apoptosis-inducing pharmacological activity against CRC *in vitro*.

### 3.2. *UAT-B triggers apoptosis in CRC cells via inhibiting the Wnt pathway*

To further elucidate the pro-apoptotic mechanisms of UAT-B, we performed RNA-Seq analysis on treated and untreated SW480 cells. This gene expression profiling revealed 1275 differentially expressed genes (fold change $\geq$1.5 and $q < 0.05$), encompassing 654 upregulated and 621 downregulated genes (Supporting Information Fig. S1A). GO enrichment analysis indicated that UAT-B influenced signaling networks associated with DNA damage, apoptotic processes, and protein metabolic regulation, including protein phosphorylation and ubiquitination (Fig. 2A). KEGG analysis suggested UAT-B affected several cancer-associated pathways, including Wnt, TNF, MAPK, and Ras (Fig. 2B).

Using multi-pathway reporter arrays, we found that UAT-B significantly decreased reporter activities for the Wnt/β-catenin, NF-κB/TNF and DNA damage pathways but did not affect the reporter activities of other cancer-related pathways, such as the Ras, MAPK and Hedgehog pathways (Fig. 2C). The Wnt signaling pathway appears to be the most significantly regulated pathway by UAT-B among all the tested pathways. Moreover, GSEA analysis and heat map representation illustrated that genes altered by UAT-B were primarily implicated in protein metabolism, Wnt signaling, and apoptosis (Fig. 2D and Fig. S1B). Given that aberrant Wnt signaling activation plays a pivotal role in colorectal tumor development and progression[22], we further examined the effect of UAT-B on Wnt signaling transcriptional activity. Selective inhibition of TOPFlash/FOPFlash reporter activity was observed in UAT-B-sensitive CRC cell lines (Fig. 2E), with a consistent downregulation of Wnt target genes *Cyclin D1* and *C-myc* mRNA expression in UAT-B-sensitive CRC cells (Fig. 2F). When β-catenin was silenced in UAT-B-sensitive cells, it partially negated the UAT-B-mediated increase in γ-$H_2AX$ expression (Fig. 2G). This in turn led to a reduction in the pro-apoptotic effects of UAT-B (Fig. 2H), suggesting the role of β-catenin in the effectiveness of UAT-B treatment. Western blot and immunofluorescence assays substantiated that UAT-B notably diminished nuclear β-catenin levels in SW480 cells (Fig. 2I and J). Additionally, *CTNNB1* mRNA levels remained unchanged post UAT-B treatment (Fig. 2K). We discovered that UAT-B-mediated β-catenin decrease occurred via polyubiquitin-dependent degradation (Fig. 2L), and that the proteasome inhibitor MG-132 obstructed UAT-B's efficacy in reducing β-catenin protein levels (Fig. 2M). Collectively, these findings confirm that UAT-B inhibits the Wnt pathway by modulating β-catenin stability in UAT-B-sensitive CRC cells.

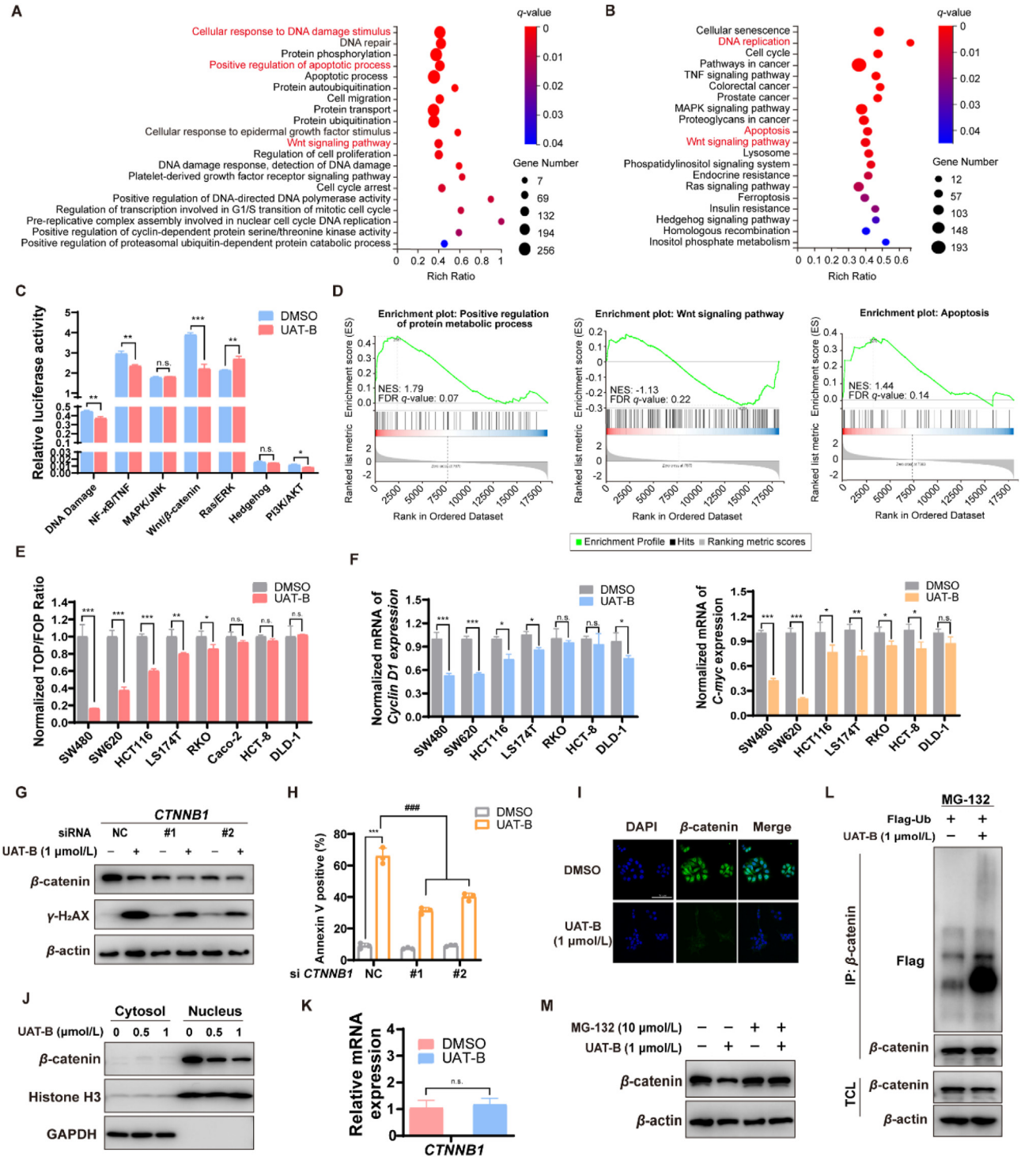


**Figure 2** UAT-B induces the apoptosis of CRC cells via inhibiting Wnt signaling. (A and B) GO (A), KEGG (B) analysis showed the differentially expressed genes (DEGs) in SW480 cell with UAT-B treatment for 3 h. (C) SW480 cells were transfected with 1 μg of plasmid, and then UAT-B (1 μmol/L) or DMSO was added and cells were cultured for 3 h. The plates were analyzed for Firefly and Renilla luciferase activities. (D) GSEA analysis showed the DEGs in protein metabolic, Wnt signaling pathway and Apoptosis. (E) CRC cells were co-transfected with TOPFlash or FOPFlash reporter. After UAT-B treatment for 6 h or not, total cell lysate was collected to measure the Firefly and Renilla luciferase activities. (F) CRC cells were treated with UAT-B for 12 h and mRNA levels of Wnt target genes were measured by qRT-PCR. (G) and (H) Effects of UAT-B (1 μmol/L) on SW480 cells transfected with *CTNNB1*-specific siRNAs (#NC or #1 or #2). In (G), Western blot analysis of β-catenin and γ-$H_2AX$, cells were treated with UAT-B for 24 h. In (H), Summary of apoptotic cells by flow cytometry assay, cells were treated with UAT-B for 48 h $^{###}P < 0.001$ *vs.* NC UAT-B group. (I) Immunofluorescence staining of β-catenin (green) in SW480 cells treated with UAT-B for 12 h. The nuclei were stained using DAPI (blue). ImageJ software was used to quantify the results (40 × magnification). Scale bars, 100 μm. (J) Nucleocytoplasmic separation analysis of β-catenin in SW480 after 6 h treatment with UAT-B. (K) qRT-PCR analysis of *CTNNB1* mRNA expression

### 3.3. UAT-B disrupts the TNKS-USP25 PPI leading to β-catenin degradation

The level of free β-catenin is precisely controlled by the β-catenin destruction complex, which is composed of the scaffold protein Axin 1, tumor suppressor APC, CK1α, and GSK-3β[23]. A co-immunoprecipitation (co-IP) assay indicated that UAT-B increased the β-catenin binding affinity to the endogenous Axin1, GSK3β, APC, and the phosphorylated β-catenin at S33, S37, and T41 (Fig. 3A). To ascertain whether UAT-B was operating at the β-catenin destruction complex level, we diminished the levels of its components (Axin1 or APC) or treated the cells with CHIR-99021, a GSK3β inhibitor. Our experiments showed that UAT-B failed to inhibit the Wnt pathway in CRC cells when the level of Axin1 was reduced (Fig. 3B, Supporting Information Fig. S2B and S2C). UAT-B stabilized the levels of endogenous Axin1 protein in both SW480 and HCT116 cells, which was an essential factor in decreasing active β-catenin levels. Moreover, Axin1 knockdown restored the levels of active β-catenin in UAT-B-treated cells to levels in DMSO-treated cells (Fig. 3C). We also found that UAT-B treatment significantly increased the abundance of Axin1-associated destruction complexes (Fig. 3D), indicating that Axin1 was essential for β-catenin degradation by forming functional destruction complexes in UAT-B-treated CRC cells. As Axin1 is usually degraded via PARsylation followed by ubiquitination[7], we analyzed the status of Axin1 in SW480 and HCT116 cells. UAT-B treatment was found to block the PARsylation/ubiquitination of Axin1, accumulation of which was promoted by MG-132 (Fig. 3E). We know that TNKS is the only PARsylating enzyme for Axin1 proteins[7]. The *in situ* proximity ligation assay (PLA) visualized that the direct interaction between TNKS and Axin1 was reduced in SW480 and HCT116 cells treated with UAT-B (Fig. 3F).

To identify the target of UAT-B in CRC cells, we conducted an enzyme activity assay and a cellular thermal shift assay (CETSA) in HCT116 and SW480 cells. We found that, compared to the DMSO control, UAT-B stabilized TNKS at denaturation temperatures ranging from 40 to 50 °C, indicating an interaction between UAT-B and TNKS within intact cells (Fig. 3G). Despite this, UAT-B didn't inhibit the enzymatic activity of TNKS 1 or 2 (Supporting Information Fig. S3). As overexpression of TNKS can also activate the Wnt pathway[24], we hypothesized that UAT-B might inhibit Wnt signaling activation induced by TNKS overexpression. Consistent with this hypothesis, we observed a marked decrease in TNKS protein levels when UAT-B and the protein synthesis inhibitor cycloheximide (CHX) were present (Fig. 3H). Furthermore, MG-132 partially restored the levels of TNKS in UAT-B-treated CRC cells, suggesting that UAT-B promotes the proteasomal degradation of TNKS (Fig. 3I).

Given that USP25 has been identified as a promoter of TNKS deubiquitination and stabilization[17], we speculated that UAT-B could induce TNKS degradation by disrupting the interaction between USP25 and TNKS. Decreased TNKS protein levels were observed in USP25-overexpressed CRC cells when treated with UAT-B (Supporting Information Fig. S4). Both co-IP and PLA experiments further revealed that UAT-B effectively blocked the interaction between USP25 and TNKS (Fig. 4A and B). Molecular docking studies were subsequently performed to investigate the binding mode of UAT-B to the TNKS fragment bearing the corresponding ARCs. As depicted in Fig. 4C and D, UAT-B occupied the portion of the binding region on ARC5 where USP25 interacted with TNKS, and three intensive hydrogen bonds were forged to stabilize this ligand−protein interaction, including Arg 836, Asn 876, and Lys 913 residues with different oxygen-containing functional groups on the UAT-B molecule. The SPR assays confirmed a direct interaction between UAT-B and the TNKS1-ARC5 domain. UAT-B bound with $TNKS1^{799-981}$ in a time-dependent saturation manner with a $K_D$ value of 46.62 μmol/L (Fig. 3C). Importantly, when mutations were introduced at residues R836A, N876A, and K913A on TNKS1-ARC5, UAT-B's binding affinity was significantly reduced for the N876A variant, leading to the loss of its ability to block the USP25/TNKS interaction (Fig. 4F and G). This conclusion is further supported by cell viability assessments using UAT-B with the TNKS1-ARC5 fragment or its N876 mutation (Fig. 4H). In molecular docking experiments, the phenolic hydroxyl group on the benzoylamine moiety of UAT-B was identified as its potential pharmacophore. To validate this hypothesis, we performed a methylation reaction to convert the phenolic hydroxyl group into a methoxy group, resulting in a UAT-B analogue called UAT-Bp (Supporting Information Scheme S1). Comparative experiments revealed that upon removal of the hydrogen bonding effect of the phenolic hydroxyl group, the binding affinity between UAT-Bp and $TNKS1^{799-981}$ significantly decreased, as evidenced by a KD value of 178 μmol/L (Fig. 4I). Overall, our findings suggest that the phenol group on the depsipeptide molecule of UAT-B, which is predicted to interact with the Asn876 in TNKS, might serve as a crucial pharmacophore. These results indicate that UAT-B could disrupting USP25-mediated stabilization and deubiquitination of TNKS, thereby encouraging Axin 1 to drive the degradation of β-catenin.

### 3.4. UAT-B inhibits TNKS-dependent Wnt pathway to overcome multi-drug resistance

To determine molecular characteristics related to cellular sensitivity towards UAT-B, we undertook an analysis of the genetic backdrop across 17 different CRC cell lines by utilizing Project Achilles[25] (www.broadinstitute.org/achilles). Our investigation revealed no discernible link between UAT-B's effects and the presence of mutations in *APC/CTNNB1*, mutations known to potentially induce abnormal activation of the Wnt pathway in CRC cells[26] Intriguingly, not all CRC cells that exhibited an abnormal Wnt pathway demonstrated a high degree of sensitivity towards UAT-B (Supporting Information Table S2). As demonstrated in Fig. 4H, the ectopic expression of TNKS-WT did, however, enhance the sensitivity of HEK-293T cells to UAT-B. An assessment of the baseline levels of TNKS was performed across a range of human CRC cell lines (Fig. 5A). It is particularly noteworthy that a higher level of TNKS protein in CRC cell lines was associated with an enhanced anti-CRC effect of UAT-B. Further analysis established a negative correlation between the $IC_{50}$ values

levels in SW480 cell line treated with 1 μmol/L UAT-B for 6 h. (L) UAT-B induced degradation of β-catenin in a proteasome-dependent manner. Flag-Ub was transiently overexpressed in SW480 cells which were treated with MG-132 for 2 h, followed by DMSO or UAT-B for 4 h. Whole-cell lysates (WCL) were shown at bottom. (M) Western blot analysis of proteasomal degradation of β-catenin in SW480 cell treated with or without MG-132 containing UAT-B for 6 h. The data represent the mean ± SD from three independent experiments. $^*P < 0.05$, $^{**}P < 0.01$, $^{***}P < 0.001$; n.s., statistically not significant.

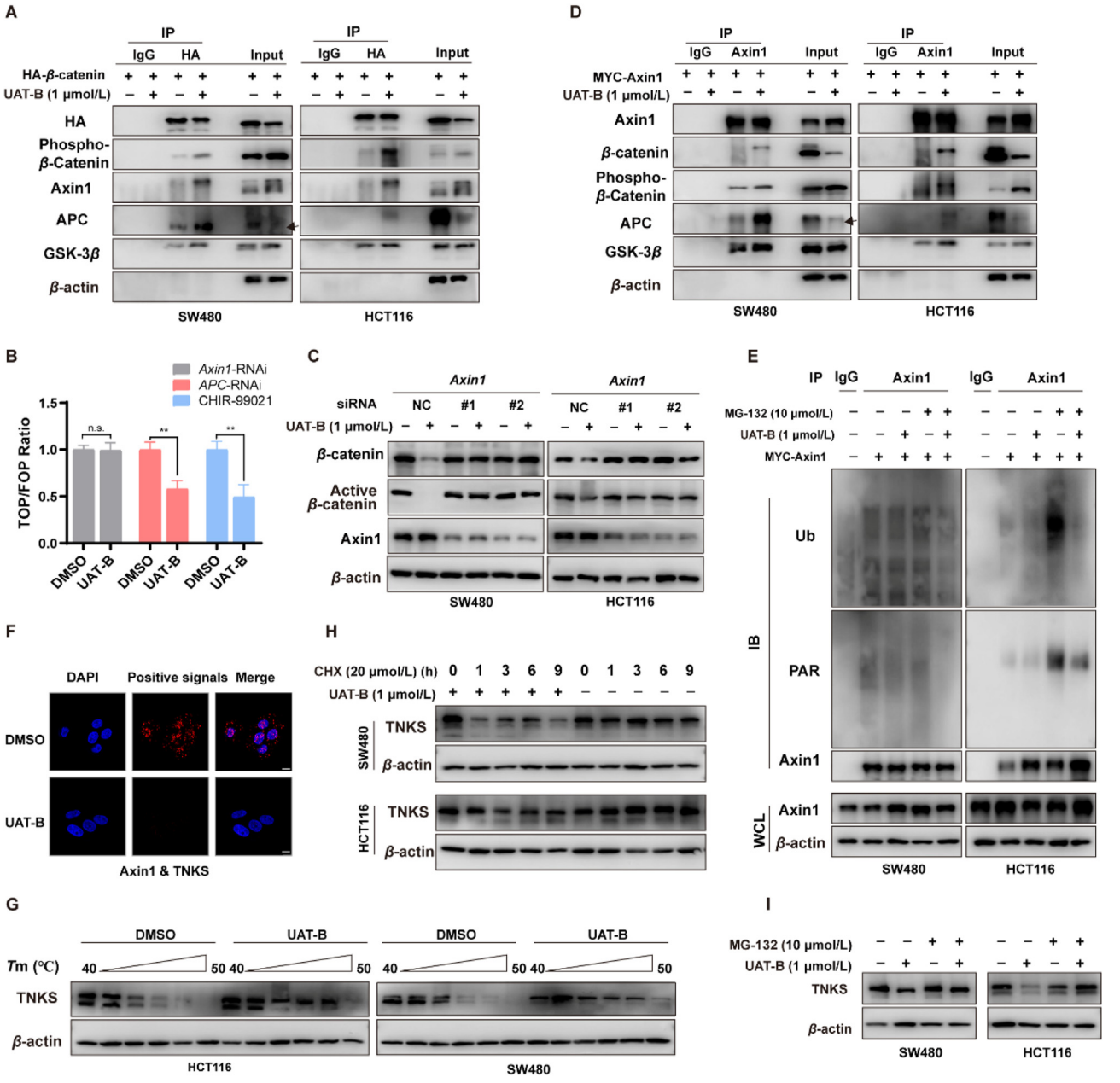


**Figure 3** UAT-B promotes TNKS degradation leading to Axin 1-directed β-catenin degradation. (A) Cells were transfected with HA-β-catenin and DMSO or UAT-B for 8 h and lysed for IP with control IgG or anti-HA antibody. The IP complexes were Western blotted for components of β-catenin destruction complexes. Arrowhead indicated a truncated APC protein. (B) HCT116 cells co-transfected with TOPFlash and FOPFlash reporter and treated with Axin1-siRNA, APC-siRNA or CHIR-99021 (2 μmol/L). After UAT-B (1 μmol/L) treatment for 6 h or not, total cell lysate was collected to measure the Firefly and Renilla luciferase activities. (C) Cells were transfected with Axin1-specific siRNAs (#1 or #2) and Western blotted for active β-catenin. (D) Cells transfected with MYC-Axin1 treated with DMSO or UAT-B for 8 h and lysed for IP with control IgG or anti-Axin1 antibody. The IP complexes were Western blotted for components of β-catenin destruction complexes. Arrowhead indicated a truncated APC protein. (E) Cells were lysed for IP with anti-Axin1 antibody. MG-132 and UAT-B were treated for 4 h before lysis. The IP complexes were Western blotted for PARsylation (PAR) and ubiquitination (Ub). (F) PLA showed direct interaction between TNKS and Axin1 proteins in SW480 cells. DAPI-stained images were merged with DuoLink red fluorescence images (Merge). Scale bar, 10 μm. (G) Western blot analysis of CETSA samples. Cells were incubated with DMSO or UAT-B (1 μmol/L) at 37 °C for 1 h before being heated at the indicated temperatures. Cells were lysed and the soluble proportions were analyzed using Western blot with indicated antibodies. (H) Western blot analysis of TNKS in CRC cells incubated with CHX and DMSO or UAT-B. (I) Western blot analysis of TNKS proteasomal degradation in SW480 cells treated with UAT-B with or without MG-132 for 6 h. Data are representative of three independent experiments. $^{**}P < 0.01$; n.s., statistically not significant.

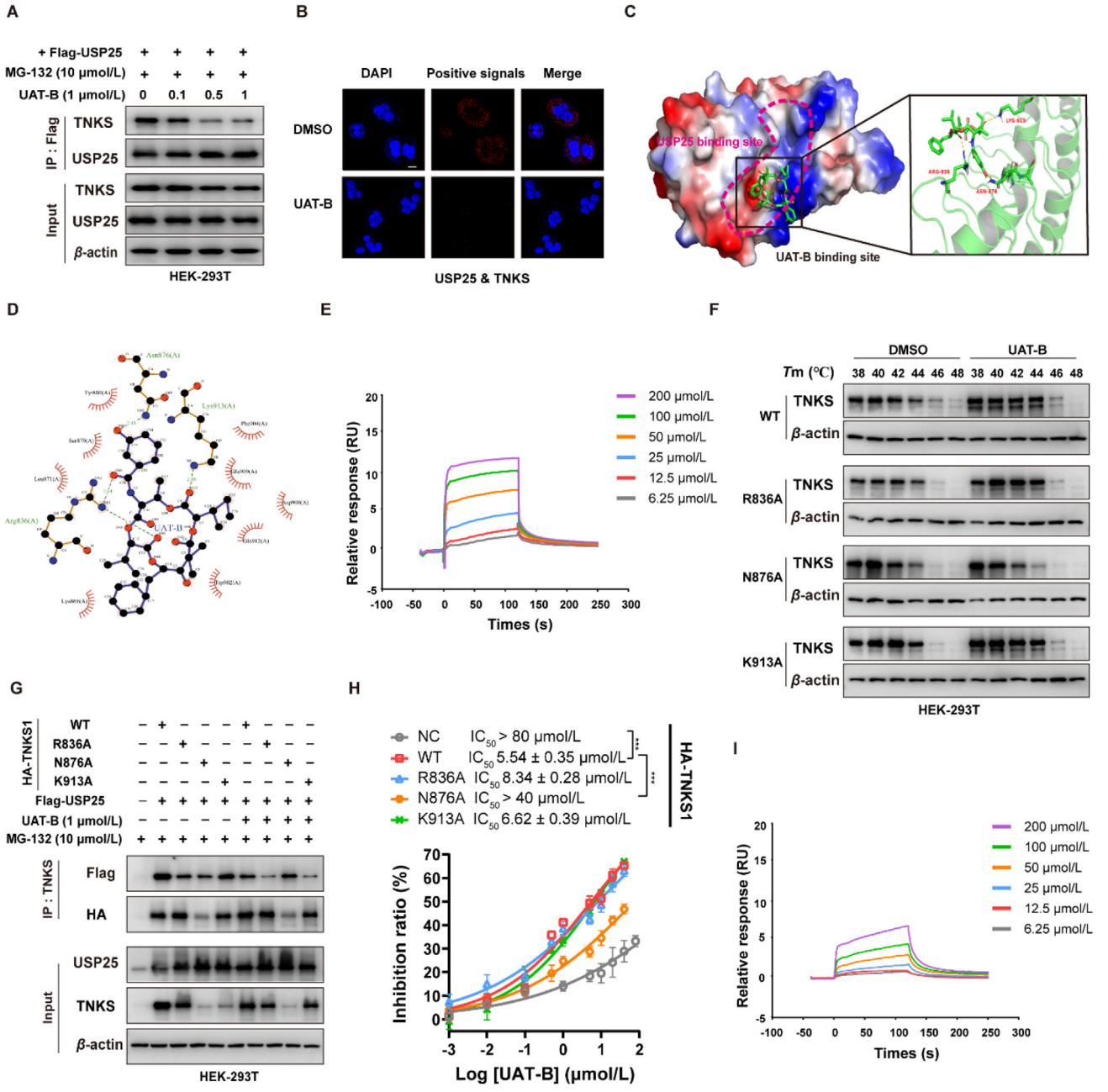


**Figure 4** UAT-B disrupts the TNKS-USP25 PPI. (A) SW480 cells transfected with Flag-USP25 were treated with DMSO or UAT-B and lysed for IP with control IgG or anti-Flag antibody. (B) PLA showed the effect of UAT-B on interaction between TNKS and USP25 in SW480 cell. Scale bar, 10 μm. (C) Overview of the UAT-B binding site on TNKS1-ARC5. Top: Overall structure with the electrostatic surface of TNKS1-ARC5 (positive: blue, negative: red, neutral: white). Inset: Detailed binding region of UAT-B. UAT-B is shown as green sticks. The residues $Arg^{836}$, $Asn^{876}$ and $Lys^{913}$ are highlighted within the stick model. (D) 2D interaction of UAT-B with TNKS1-ARC5. (E) Surface plasmon resonance (SPR) analyses of the kinetic interaction between UAT-B and TNKS-ARC5 domain. (F)—(H) The plasmids of HA-TNKS1 (WT, R836A, N876A or K913A) were transfected in HEK-293T cells and then treated with indicated concentrations of UAT-B. In (F), Western blot analysis of CETSA samples. In (G), cells were simultaneously transfected with Flag-USP25 and lysed for co-IP. In (H), the inhibition of cell viability was measured after UAT-B 24 h treatment. (I) SPR analyses of the kinetic interaction between UAT-Bp and TNKS-ARC5 domain. Data are representative of three independent experiments. ***$P < 0.001$; n.s., statistically not significant.

of UAT-B and the protein levels of TNKS in CRC cell lines (Pearson correlation, $r = -0.7459$, $P = 0.0034$, $n = 13$) (Fig. 5B).

TNKS is thought to potentially serve as a promising scaffold that promotes the Wnt pathway, independent of its PARP activity[27]. Our study found that when TNKS was directly inhibited with a specific inhibitor, G007-LK, the protein levels of TNKS increased. However, there were no observable changes in the protein levels of active β-catenin or the Wnt target proteins C-myc and Cyclin D1 (Fig. 5C). These findings suggest that simply

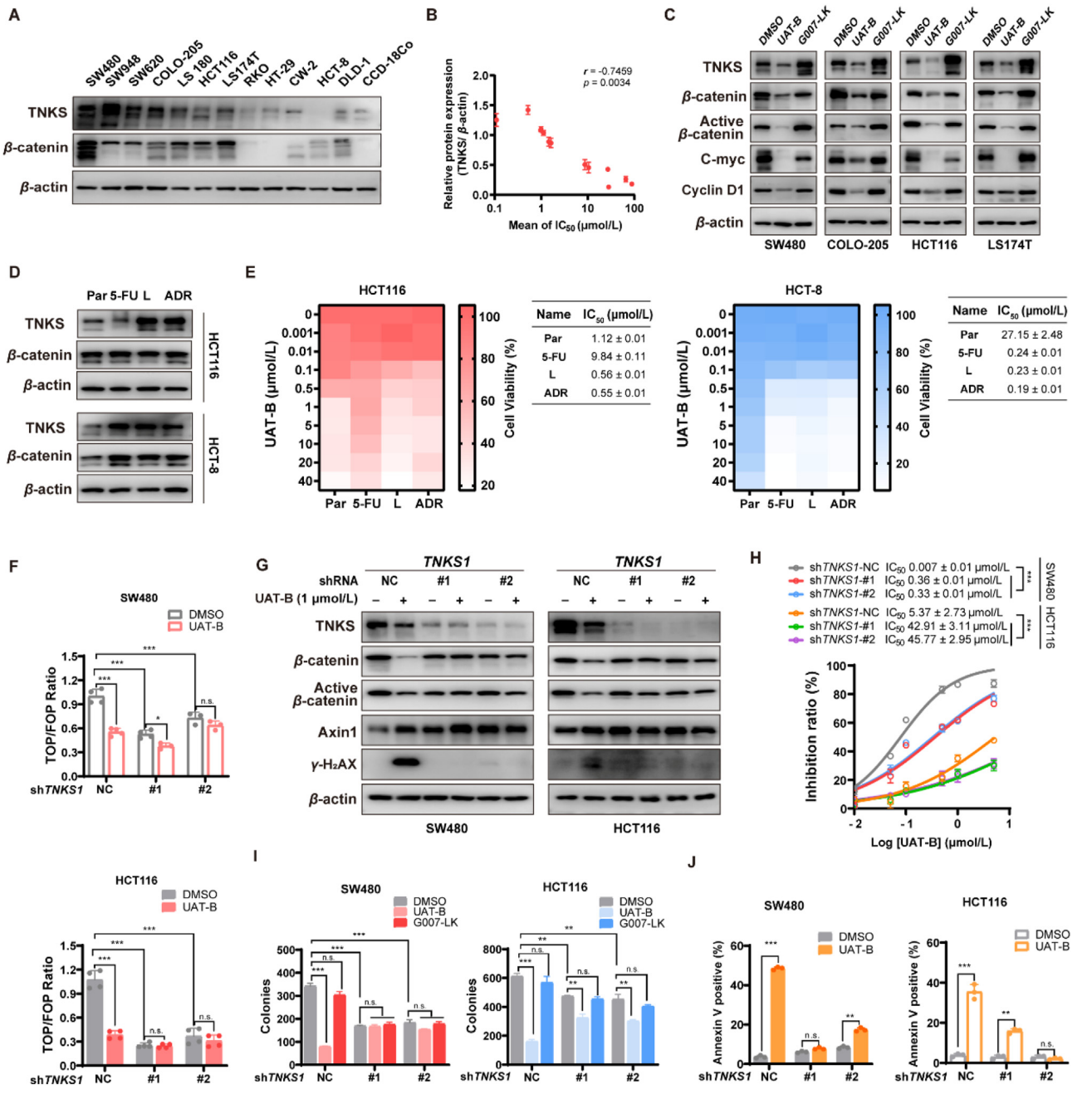


**Figure 5** UAT-B overcomes multi-drug resistance of TNKS-overexpressing CRC cells through inhibiting the TNKS-dependent Wnt pathway. (A) Representative Western blots of TNKS expression in a non-malignant cell and twelve CRC cell lines. (B) Correlation analysis of the TNKS percentage relative to that of $\beta$-actin with $IC_{50}$ values of UAT-B at 48 h. The TNKS level and $IC_{50}$ value of UAT-B were subjected to Pearson correlation analysis ($r = -0.7459$, $P = 0.0034$, $n = 13$). (C) Representative Western blots of TNKS and Wnt pathway-related proteins in CRC cells with high levels of TNKS treated with UAT-B or G007-LK. (D) Representative Western blots of TNKS and $\beta$-catenin protein expression in chemotherapy drugs-resistant CRC cells and their parental counterparts. (E) Inhibition effects of UAT-B on chemotherapy drugs-resistant CRC cells and their parental counterparts assayed by CCK-8. Cells were treated with the indicated concentration of UAT-B for 48 h. (F)−(J) Effects of UAT-B on TNKS1 knockdown CRC cells and their parental counterparts (TNKS1-#1, TNKS1-#2 or TNKS1-NC). In (F), TOPFlash/FOPFlash reporter activity assayed by Dual-Luciferase Reporter Assay System, cells were treated with UAT-B (1 μmol/L) for 6 h. In (G), Western blot of TNKS, Wnt/$\beta$-catenin signaling pathway-related proteins and $\gamma$-$H_2AX$, cells were treated with UAT-B (1 μmol/L). In (H), cell viability assay by CCK-8, cells exposed to UAT-B for 24 h. In (I), colony formation assay and summaries of colony numbers in cells treated with 1 μmol/L UAT-B, DMSO or 10 μmol/L G007-LK and cultured for 10 days. In (J), Summary of apoptotic cells by flow cytometry assay, cells were treated with UAT-B (1 μmol/L) for 24 h. The data represent the mean ± SD from three independent experiments. *$P < 0.05$, **$P < 0.01$, ***$P < 0.001$; n.s., statistically not significant.

**Table 1** $IC_{50}$ (μmol/L) values in TNKS-overexpression CRC cell lines.

| Cell lines | 5-FU[a] | Oxaliplatin[a] | G007-LK[a] | XAV939[a] |
|---|---|---|---|---|
| SW480 | >40 | 22.23 ± 3.82 | >40 | >40 |
| LoVo | 18.34 ± 1.57 | 5.38 ± 0.18 | 15.92 ± 1.44 | >40 |
| SW948 | >40 | >40 | >40 | >40 |
| SW620 | >40 | >40 | >40 | >40 |
| COLO-205 | 4.83 ± 0.21 | 4.39 ± 0.29 | >40 | >40 |
| LS 180 | >40 | >40 | >40 | >40 |
| HCT116 | 10.73 ± 0.23 | 6.17 ± 1.11 | >40 | >40 |
| LS 174T | >40 | >40 | >40 | >40 |
| COLO-320 DM | >40 | >40 | 23.33 ± 1.41 | >40 |
| T84 | >40 | 36.88 ± 2.39 | >40 | >40 |

[a]The $IC_{50}$ ± SD values of 5-FU, Oxaliplatin, G007-LK and XAV939 to the indicated CRC cell lines were determined by CCK-8 assay. The data represent the mean ± SD from three independent experiments.

inhibiting the catalytic activity of TNKS may not be sufficient to suppress Wnt activity in CRC cells with high TNKS levels. To investigate the association between TNKS levels and drug resistance, we evaluated the growth-inhibitory effects of TNKSi (G007-LK and XAV939) and chemotherapy drugs (5-FU and oxaliplatin) on 10 CRC cell lines characterized by high TNKS levels. As expected, nearly all cell lines exhibiting high TNKS expression displayed resistance to both TNKSi and chemotherapeutic drugs (Table 1). Meanwhile, we generated chemotherapy drug-resistant CRC cell lines of clinical relevance, as detailed in the Materials and Methods section (Supporting Information Fig. S5A and Table S3). Excluding HCT116/5-FU cells, the expression levels of TNKS in chemotherapy drug-resistant CRC cells were higher than those in parental cells (Fig. 5D). In the acquired drug-resistant cell lines, we noted that UAT-B exerted inhibitory effects on Wnt transcriptional activity (Fig. S5B) and reduced the expression of TNKS and Wnt target proteins (Fig. S5C). As a result of this inhibition, there was a significant suppression of cell proliferation (Fig. S5D), coupled with an induction of apoptosis (Fig. S5E).

Next, we confirmed that the differential sensitivity of CRC cells to UAT-B was due to the aberrant Wnt pathway dependent on TNKS. UAT-B notably inhibited the protein expression of TNKS and various components of the Wnt pathway in CRC cells exhibiting high TNKS levels (Fig. 5C). CRC cells resistant to chemotherapy and characterized by high TNKS levels showed greater sensitivity to UAT-B compared to the parent cells (Fig. 5E). Depletion of endogenous TNKS hindered the UAT-B-induced inhibition of TOPFlash/FOPFlash reporter activity and β-catenin degradation (Fig. S5, Fig. 5F and G). Concurrently, reductions in cell viability and *in-vitro* colony formation prompted by UAT-B were nearly negated by TNKS depletion (Fig. 5H and I). A decrease in cell viability was also observed in TNKS-depleted cells when compared to control vector-transfected cells (Fig. 5I). Furthermore, UAT-B did not trigger apoptosis in TNKS-depleted cells (Fig. 5J). Therefore, these observations indicated that UAT-B-sensitive CRC cells display two characteristic features: (i) high-levels of TNKS, and (ii) a TNKS-dependent aberrant Wnt pathway.

### 3.5. *UAT-B suppresses MDR CRC progression in vivo*

In order to explore the *in vivo* antitumor activity of UAT-B, we established xenograft mouse models using SW480 and RKO cells (Fig. 6A). The SW480 CDX model, which exhibits high TNKS expression, UAT-B significantly suppressed xenograft growth in a dose-dependent manner, exhibiting a T/C ratio of 46.24 ± 2.54% at 0.5 mg/kg and 22.96 ± 3.56% at 1 mg/kg. In contrast, G007-LK and 5-FU failed to restrain tumor growth (Fig. 6B and C, Supporting Information Fig. S7A). UAT-B treatment also significantly reduced the weight of SW480 tumors in the xenograft mouse model by 70%, while G007-LK and 5-FU treatments led to a 30% inhibition of tumor growth (Fig. 6C). In the RKO CDX model, characterized by a lower expression level of TNKS, UAT-B did not affect the growth of RKO-driven tumors (0.5 mg/kg, T/C ratio of 89.55 ± 6.62% and 1 mg/kg, T/C ratio of 90.50 ± 5.87%), consistent with the effects observed for G007-LK (20 mg/kg, T/C ratio of 99.23 ± 4.32%) and 5-FU (20 mg/kg, T/C ratio of 60.88 ± 2.40%) (Fig. 6B and C, Fig. S7A). H&E staining exhibited pronounced tumor necrosis in UAT-B-treated SW480 xenografts as compared to RKO xenografts (Fig. 6D). IHC and Western blot analyses of xenograft tissues confirmed TNKS and β-catenin degradation mediated by UAT-B in SW480, but not in RKO xenografts, corroborating our *in vitro* observations. Additionally, we found that levels of C-myc and Cyclin D1 were suppressed by UAT-B in TNKS-overexpressing tumors (Fig. 6D and E, Fig. S7B). γ-$H_2$AX expression levels and the proportion of apoptotic cells was also notably increased in SW480, but not RKO tumor xenografts treated with UAT-B (Fig. 6E and F). These data suggest that UAT-B has the potential to induce TNKS degradation and disrupt the Wnt signaling pathway, thereby counteracting multidrug resistance in TNKS-overexpressing CRC cells *in vivo*.

Considering the superior activity of UAT-B against MDR cancer cells, we investigated the *in vivo* antitumor activity of UAT-B in a xenograft mouse model established with HCT-8/5-FU cells (Fig. 6G). Remarkably, UAT-B, either administered alone (1 mg/kg, T/C ratio of 18.22 ± 2.99%) or in conjunction with 5-FU (UAT-B 0.5 mg/kg + 5-FU 10 mg/kg, T/C ratio of 17.98 ± 2.73%), effectively delayed tumor growth and without significant body weight loss or gross signs of toxicity (Fig. S7F and Supporting Information Fig. S9A−S9D). On the contrary, G007-LK, both alone (20 mg/kg, T/C ratio of 74.70 ± 8.98%) and combined with 5-FU (G007-LK 10 mg/kg + 5-FU 10 mg/kg, T/C ratio of 74.68 ± 5.48%), failed to suppress tumor growth (Fig. 6H and I, Fig. S7C). UAT-B, whether applied alone or in combination with 5-FU, notably inhibited the expression of TNKS and β-catenin (Fig. 6J and Fig. S7D) and boosted apoptosis (Fig. 6K and Fig. S7E). UAT-B exhibits profound antitumor efficacy *in vivo* against acquired MDR CRC tumors with high TNKS levels.

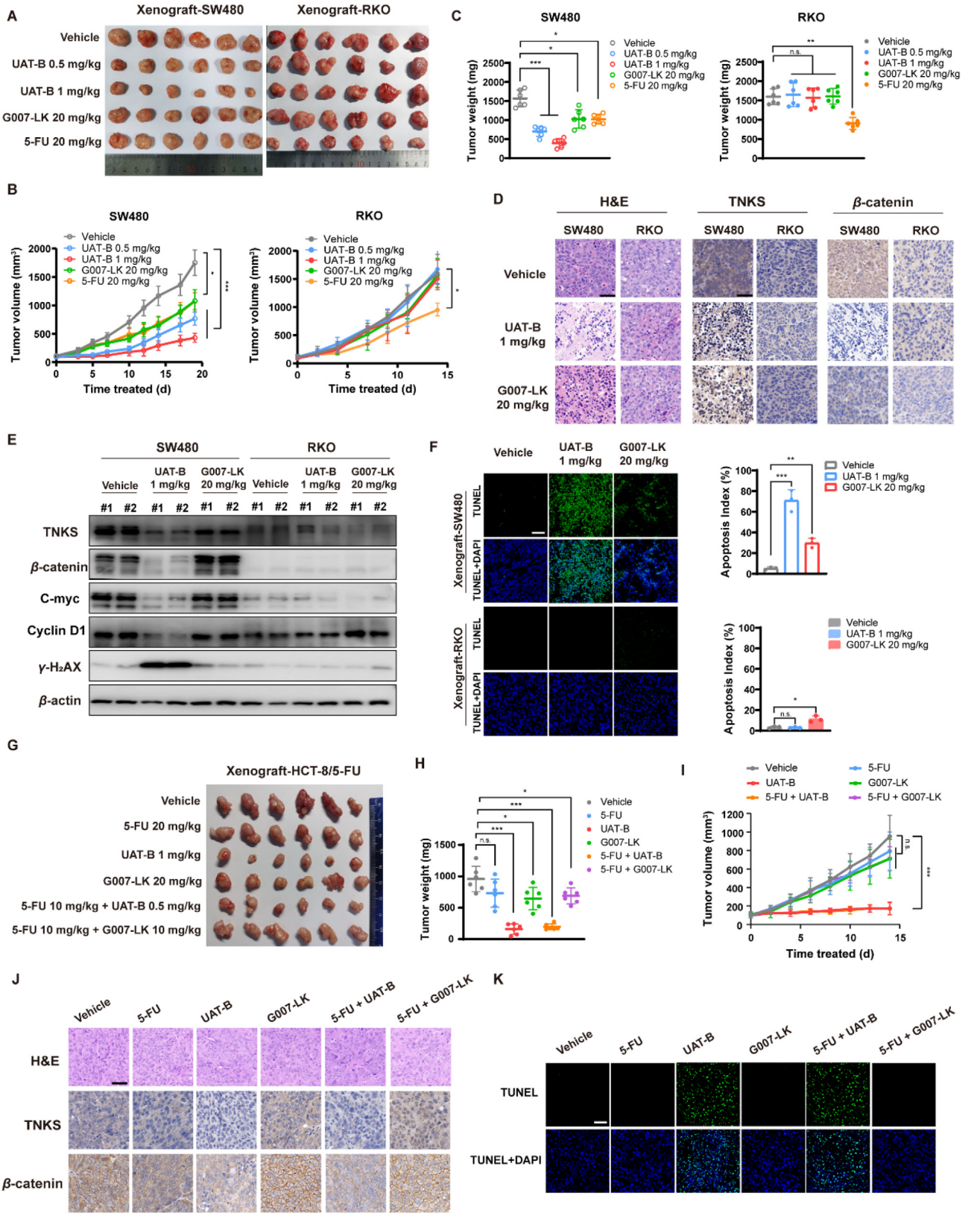


**Figure 6** UAT-B exhibits potency in MDR tumors with high level of TNKS. (A)−(C) SW480-CDX tumors and RKO-CDX tumors treated with UAT-B, G007-LK and 5-FU shown in image (A), tumor growth (B), and weight change (C) analysis. The CDX-bearing mice were treated with vehicle or with 0.5 or 1 mg/kg UAT-B or with 20 mg/kg G007-LK or with 20 mg/kg 5-FU every day for 16 days. (D) Representative tissue sections from SW480 and RKO xenograft tumors with H&E and IHC staining in different groups of mice. Scale bars, 50 μm. (E) Representative Western blot analysis in each group of CDX tumors. (F) TUNEL (green) staining in different groups of mice. The nuclei were stained using DAPI (blue). Scale bars, 50 μm. ImageJ software was used to quantify the results. Results were shown as mean ± SEM of $n = 5$ mice per group. (G)−(I) HCT-8/5-FU-CDX

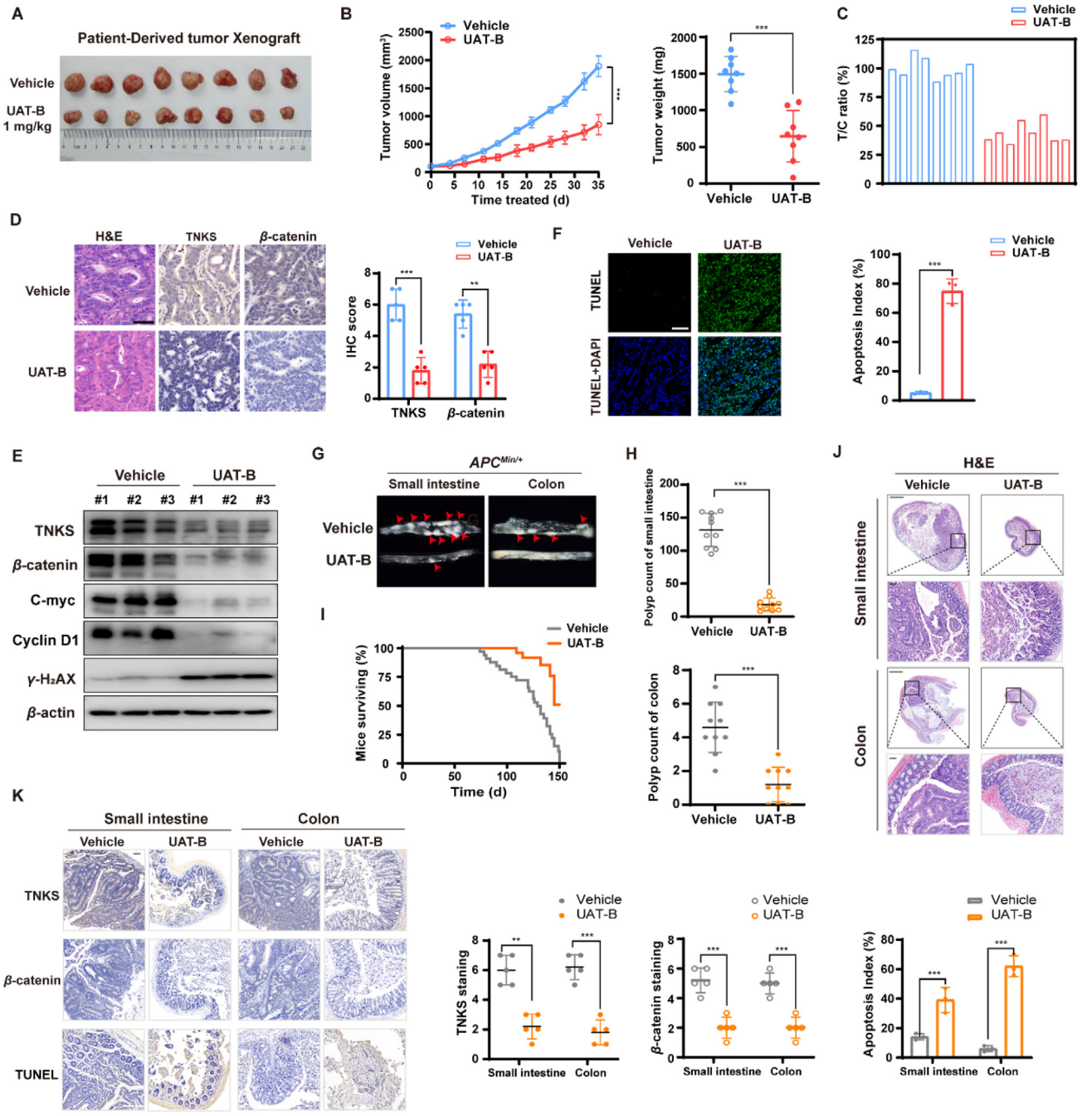


**Figure 7** UAT-B suppresses tumorigenesis and progression in PDX and $APC^{min/+}$ spontaneous CRC models. (A)−(C) Patient-derived xenograft (PDX) tumor treated with UAT-B (1 mg/kg, once daily) for 35 days shown in image (A), tumor growth (B, left panel), weight change (B, right panel), and T/C ratio (C) analysis. $n = 8$ mice per group. (D)−(F) Representative tissue sections from PDX tumors with H&E and IHC staining analysis (D), Western blot analysis (E) and TUNEL staining analysis (F). Scale bars, 50 μm. (G)−(I) Effects of UAT-B (1 mg/kg, every other day) treatment on $APC^{min/+}$ spontaneous CRC models shown as photomicrographs of the small intestine and colon tissues (G), macroscopic polyps (>3 mm in diameter) in the small intestine (H, upper panel) and colon tissues (H, lower panel) ($n = 10$ mice per group, 70 days, repeated-measures ANOVA) and Kaplan−Meier survival analysis ($n = 20$, 150 days) (I). (J) Cross sections of frozen small intestines and colons were stained by H&E. (4 × magnification; Scale bars, 500 μm. or 20× magnification; Scale bar, 50 μm). (K) Representative tissue sections from $APC^{Min/+}$ mice with IHC staining analysis. Scale bars, 50 μm. *P* values were determined using two-way ANOVA with Tukey multiple comparison test. $^{**}P < 0.01$, $^{***}P < 0.001$.

tumors treated with UAT-B, G007-LK, 5-FU and UAT-B and G007-LK combined with 5-FU respectively shown in image (G), weight change (H), and tumor growth (I) analysis. $n = 6$ mice per group. (J) Representative tissue sections from HCT-8/5-FU xenograft tumors with H&E and IHC staining in different groups of mice. Scale bars, 50 μm. (K) TUNEL (green) staining in different groups of mice. The nuclei were stained using DAPI (blue). Scale bars, 20 μm. *P* values were determined by one-way ANOVA, $^{*}P < 0.05$, $^{**}P < 0.01$, $^{***}P < 0.001$; n.s., statistically not significant.

The therapeutic potential of UAT-B against cancer was validated using a highly clinically pertinent patient-derived xenograft (PDX) model, a tool that closely mimics primary tumors and is frequently employed for evaluating anticancer drug responses[28]. A particular PDX model, CR3079, established from a tumor excised from a colorectal cancer patient, exhibited resistance to 5-FU (Supporting Information Fig. S8). Upon UAT-B administration, the PDX tumors displayed signs of growth inhibition and a notable reduction in volume (T/C ratio of 38.45 ± 3.22%) (Fig. 7A–C), accompanied by a decrease in TNKS and $\beta$-catenin levels (Fig. 7D and E). Immunoblot assays further corroborated these observations, showing that UAT-B treatment considerably suppressed $\beta$-catenin and its transcriptional targets, C-myc and Cyclin D1, and augmented $\gamma$-$H_2AX$ levels (Fig. 7E), along with an increase in TUNEL-positive apoptotic cells (Fig. 7F). In $APC^{Min/+}$ mice, models of spontaneous CRC, UAT-B treatment yielded a significant reduction in the number and size of discernible intestinal polyps (Fig. 7G and H), while also extending the mice's lifespan compared to the control group (Fig. 7I). Histopathological assessment further affirmed that UAT-B decreased the prevalence and size of adenomatous polyps, a type of pre-cancerous lesion (Fig. 7J). Moreover, UAT-B treatment resulted in a decline in the levels of TNKS and $\beta$-catenin proteins and an increase in apoptosis within the polyps (Fig. 7K). Taken together, our findings strongly suggest that UAT-B manifests potent pharmacological inhibition against MDR colorectal cancer *in vivo*.

## 4. Discussion

Currently, there are limited options for targeted therapies for advanced and recurrent CRC, with the inhibition of vascular endothelial growth factor (VEGF) and epidermal growth factor receptor (EGFR) being among the few available options[29,30]. Consequently, there is an urgent need for novel targeted therapeutics for treating resistant CRC. While TNKS has emerged as a potential target in anti-CRC therapy, concerns have arisen over whether its inhibitory activity alone is sufficient to suppress the Wnt signaling activity in TNKS overexpressing cancer cells[7,27]. Given that USP25 controls the stability of TNKS through deubiquitination, interrupting the interaction between USP25 and the ankyrin repeats in TNKS presents a unique opportunity. This approach could stabilize Axin 1 and inhibit Wnt signaling by promoting TNKS degradation, as opposed to inhibiting their enzymatic activities. To date, however, only a few compounds have been identified that can target the protein–protein interactions between TNKS and USP25[31].

UAT-B, a novel neoantimycin analog, is a 15-membered ring antimycin-type depsipeptide[20]. Neoantimycin (NAT) derivatives and their analogs have long been recognized for their immunosuppressive, antimicrobial, fungicidal, and antitumor properties[19]. Our previous work demonstrated that NAT derivatives displayed stronger inhibitory effects than cisplatin, and further investigations found that NAT-F induced mitochondria-related apoptosis in human non-small cell lung cancer cells[32,33]. As for UAT-B, it exhibits remarkable anticancer activity akin to other NAT derivatives, but notably without apparent toxicity to colon epithelial cells[20]. In the current study, we discovered that UAT-B preferentially induces apoptosis in MDR colorectal cancer through the inhibition of the Wnt pathway. This apoptotic effect of UAT-B was consistently observed from cell line-based assays to four robust preclinical models, including patient-derived organoid, patient-derived xenograft, and $APC^{min/+}$ spontaneous colorectal cancer models, and was positively correlated with the level of TNKS.

TNKS is highly expressed in various types of cancers, including colorectal, breast, lung, gastric, and ovarian cancers, and has emerged as a potential therapeutic target for a range of Wnt pathway-dependent cancers[34,35]. Our study uncovers that elevated levels of TNKS contribute to chemotherapeutic drug resistance in colorectal cancer cells and mouse xenografts. This suggests that TNKS levels could serve as a significant indicator for the detection of chemotherapeutic drug resistance in CRC patients. We also observed that a sustained increase in TNKS expression coincided with long-term administration of chemotherapy drugs in the drug-resistant cell line we constructed, with the exception of the HCT116/5-FU cell line. Interestingly, UAT-B was able to overcome the acquired resistance to 5-FU, oxaliplatin, and adriamycin in colorectal cancer tumors that overexpress TNKS. These findings present the first pharmacological evidence that overexpression of TNKS is a marker of chemoresistance in colorectal cancer, positioning UAT-B as a promising small molecule to counteract multi-drug resistance in TNKS-overexpressing CRC. However, the mechanism by which TNKS mediates insensitivity to chemotherapeutic drugs remains elusive and necessitates further investigation.

The structure of TNKS includes five ankyrin (ANK) repeats, a sterile alpha motif (SAM), and a carboxy-terminal PARP catalytic domain[36]. To date, more than 20 relatively novel small-molecule TNKS inhibitors, such as XAV939[37], IWR-1 and IWR-2[38], RK-287107[39], JW55[40] and JW74[41], and its derivative G007-LK[42], have been reported. These inhibitors target the catalytic domain to suppress the poly (ADP-ribosyl) ation function of TNKS[35]. However, our study reveals that XAV939 and G007-LK could not suppress Wnt activity in CRC with high levels of TNKS, which exhibited multi-drug resistance (Fig. 5C and Table 1). Previous studies have found that the accumulation of TNKS as a compensatory response against TNKS catalytic inhibition leads to insensitivity to TNKS inhibitors, posing significant obstacles to the clinical development of these molecules[35]. Interestingly, the TNKS–USP25 complex may provide an attractive target. USP25 interacts with TNKS through ankyrin repeats, a feature not present in other members of the PARP family, thus potentially avoiding unnecessary toxicity. Notably, USP25 mRNA levels are significantly elevated in cancer tissues compared to adjacent tissues, providing a potential therapeutic window[43–45]. Our study introduces UAT-B, a novel inhibitor of protein–protein interactions, that targets ARC5 of TNKS1, thereby significantly enhancing the specificity of TNKS inhibition. Crystal structure analysis demonstrated that the Asn 876 residue of TNKS1 is important for the interaction between TNKS1 and USP25[17]. In line with this, we found that the Asn876 residue of TNKS1 is critical for the inhibition of TNKS–USP25 binding by UAT-B (Fig. 4F). Consequently, the development of small molecules targeting the TNKS1–USP25 protein–protein interaction to stabilize Axin 1 by promoting the degradation of TNKS, rather than inhibiting its enzymatic activities, appears to be an effective strategy to counteract multi-drug resistance in TNKS-overexpressing CRC.

Natural products featuring privileged scaffolds hold significant potential for the design of molecular probes and the development of drugs. Nonetheless, identifying their molecular targets is often a formidable challenge. In our study, we've provided a practical method that combines transcriptomics with cellular profiling to facilitate target identification. We've discovered that the natural depsipeptide UAT-B interacts with the ARC5 subunit of TNKS at

the Asn 876 residue. UAT-B could, therefore, serve as a versatile tool for examining the biology of the TNKS-US25 protein−protein interaction. Indeed, UAT-B could be considered a promising lead candidate for developing treatments against CRC, particularly for those cases that exhibit high levels of TNKS and resistance to multiple drugs.

## 5. Conclusions

In summary, this is the first study to suggest that TNKS degradation by UAT-B has a more significant effect than inhibiting the catalysis of TNKS in multi-drug resistance CRC with high TNKS levels. It highlights a promising lead compound, UAT-B, that could support future preclinical and clinical applications in TNKS-overexpressing CRC treatment. Additionally, this research suggests that TNKS overexpression might serve as a predictive marker for chemotherapy resistance in CRC patients.

## Acknowledgments

This study was financially supported by the National Key Research and Development Program of China (2022YFC2804100, 2021YFF0502400, 2022YFC2804300); National Natural Science Foundation of China (82073713, 22137006, 82104033, 82173730, 81903499, 32070070, 82160669); Innovative research team of high-level local universities in Shanghai (SHSMU-ZDCX20212702, China). We thank Dr. Juncheng Su from Shanghai Jiao-Tong University School of Medicine (Shanghai, China) for providing the LoVo and COLO 320DM cell lines.

## Author contributions

Houwen Lin and Fan Sun were the principal architects of the project, devising the experimental design and overseeing manuscript revisions. Collaboratively, Hongrui Zhu, Yamin Gao, and Liyun Liu were pivotal in the experimental planning, data integration, and authoring of the manuscript. Mengyu Tao and Li Liu performed PDO studies and cell-based assays. Hongze Liao and Xiao Lin performed Docking analysis. Yaoyao Shen, Yijia Cheng and Yongjun Zhou helped perform compound synthesis. Haitao Xue contributed significantly to the structural modification of the compound under study. Li Guan and Huimin Zhao contributed substantially to the execution of the *in vivo* experiments. Fan Yang and Shuping Wang helped to touch up the manuscript. All other authors contributed specific parts of the manuscript.

## Conflicts of interest

The authors declare no potential conflicts of interest.

## Appendix A. Supporting information

Supporting data to this article can be found online at https://doi.org/10.1016/j.apsb.2023.10.013.

## References

1. Siegel RL, Miller KD, Goding Sauer A, Fedewa SA, Butterly LF, Anderson JC, et al. Colorectal cancer statistics, 2020. *CA Cancer J Clin* 2020;**70**:145−64.
2. Szakacs G, Paterson JK, Ludwig JA, Booth-Genthe C, Gottesman MM. Targeting multidrug resistance in cancer. *Nat Rev Drug Discov* 2006;**5**:219−34.
3. Cancer Genome Atlas N. Comprehensive molecular characterization of human colon and rectal cancer. *Nature* 2012;**487**:330−7.
4. Mehta CC, Bhatt HG. Tankyrase inhibitors as antitumor agents: a patent update (2013−2020). *Expert Opin Ther Pat* 2021;**31**:645−61.
5. Duarte D, Vale N. Combining repurposed drugs to treat colorectal cancer. *Drug Discov Today* 2022;**27**:165−84.
6. Anastas JN, Moon RT. WNT signalling pathways as therapeutic targets in cancer. *Nat Rev Cancer* 2013;**13**:11−26.
7. Riffell JL, Lord CJ, Ashworth A. Tankyrase-targeted therapeutics: expanding opportunities in the PARP family. *Nat Rev Drug Discov* 2012;**11**:923−36.
8. Morrone S, Cheng Z, Moon RT, Cong F, Xu W. Crystal structure of a Tankyrase-Axin complex and its implications for Axin turnover and Tankyrase substrate recruitment. *Proc Natl Acad Sci U S A* 2012;**109**:1500−5.
9. Kang DH, Lee DJ, Lee S, Lee SY, Jun Y, Kim Y, et al. Interaction of tankyrase and peroxiredoxin II is indispensable for the survival of colorectal cancer cells. *Nat Commun* 2017;**8**:40.
10. Yang E, Tacchelly-Benites O, Wang Z, Randall MP, Tian A, Benchabane H, et al. Wnt pathway activation by ADP-ribosylation. *Nat Commun* 2016;**7**:11430.
11. Okada-Iwasaki R, Takahashi Y, Watanabe Y, Ishida H, Saito J, Nakai R, et al. The discovery and characterization of K-756, a novel Wnt/beta-Catenin pathway inhibitor targeting tankyrase. *Mol Cancer Ther* 2016;**15**:1525−34.
12. Mizutani A, Yashiroda Y, Muramatsu Y, Yoshida H, Chikada T, Tsumura T, et al. RK-287107, a potent and specific tankyrase inhibitor, blocks colorectal cancer cell growth in a preclinical model. *Cancer Sci* 2018;**109**:4003−14.
13. Li N, Wang Y, Neri S, Zhen Y, Fong LWR, Qiao Y, et al. Tankyrase disrupts metabolic homeostasis and promotes tumorigenesis by inhibiting LKB1-AMPK signalling. *Nat Commun* 2019;**10**:4363.
14. De la Roche M, Ibrahim AE, Mieszczanek J, Bienz M. LEF1 and B9L shield beta-catenin from inactivation by Axin, desensitizing colorectal cancer cells to tankyrase inhibitors. *Cancer Res* 2014;**74**:1495−505.
15. Mariotti L, Pollock K, Guettler S. Regulation of Wnt/beta-catenin signalling by tankyrase-dependent poly(ADP-ribosyl)ation and scaffolding. *Br J Pharmacol* 2017;**174**:4611−36.
16. Reyes-Turcu FE, Ventii KH, Wilkinson KD. Regulation and cellular roles of ubiquitin-specific deubiquitinating enzymes. *Annu Rev Biochem* 2009;**78**:363−97.
17. Xu D, Liu J, Fu T, Shan B, Qian L, Pan L, et al. USP25 regulates Wnt signaling by controlling the stability of tankyrases. *Genes Dev* 2017;**31**:1024−35.
18. Haikarainen T, Krauss S, Lehtio L. Tankyrases: structure, function and therapeutic implications in cancer. *Curr Pharm Des* 2014;**20**:6472−88.
19. Liu J, Zhu X, Kim SJ, Zhang W. Antimycin-type depsipeptides: discovery, biosynthesis, chemical synthesis, and bioactivities. *Nat Prod Rep* 2016;**33**:1146−65.
20. Shen Y, Sun F, Zhang L, Cheng Y, Zhu H, Wang SP, et al. Biosynthesis of depsipeptides with a 3-hydroxybenzoate moiety and selective anticancer activities involves a chorismatase. *J Biol Chem* 2020;**295**:5509−18.
21. Driehuis E, Kretzschmar K, Clevers H. Establishment of patient-derived cancer organoids for drug-screening applications. *Nat Protoc* 2020;**15**:3380−409.
22. Zhan T, Rindtorff N, Boutros M. Wnt signaling in cancer. *Oncogene* 2017;**36**:1461−73.
23. Sferrazza G, Corti M, Brusotti G, Pierimarchi P, Temporini C, Serafino A, et al. Nature-derived compounds modulating Wnt/beta-catenin pathway: a preventive and therapeutic opportunity in neoplastic diseases. *Acta Pharm Sin B* 2020;**10**:1814−34.
24. Chen Y, Chen M, Deng K. Blocking the Wnt/beta-catenin signaling pathway to treat colorectal cancer: strategies to improve current therapies. *Int J Oncol* 2023;**62**:24.

25. Wong CC, Qian Y, Li X, Xu J, Kang W, Tong JH, et al. SLC25A22 promotes proliferation and survival of colorectal cancer cells with KRAS mutations and xenograft tumor progression in mice *via* intracellular synthesis of aspartate. *Gastroenterology* 2016;**151**:945−960 e6.
26. Bugter JM, Fenderico N, Maurice MM. Mutations and mechanisms of WNT pathway tumour suppressors in cancer. *Nat Rev Cancer* 2021; **21**:5−21.
27. Mariotti L, Templeton CM, Ranes M, Paracuellos P, Cronin N, Beuron F, et al. Tankyrase requires SAM domain-dependent polymerization to support Wnt-beta-Catenin signaling. *Mol Cell* 2016;**63**: 498−513.
28. Aparicio S, Hidalgo M, Kung AL. Examining the utility of patient-derived xenograft mouse models. *Nat Rev Cancer* 2015;**15**:311−6.
29. Kasi PM, Grothey A. Chemotherapy maintenance. *Cancer J* 2016;**22**: 199−204.
30. Dienstmann R, Vermeulen L, Guinney J, Kopetz S, Tejpar S, Tabernero J. Consensus molecular subtypes and the evolution of precision medicine in colorectal cancer. *Nat Rev Cancer* 2017;**17**: 79−92.
31. Cheng H, Li X, Wang C, Chen Y, Li S, Tan J, et al. Inhibition of tankyrase by a novel small molecule significantly attenuates prostate cancer cell proliferation. *Cancer Lett* 2019;**443**:80−90.
32. Liu L, Zhu H, Wu W, Shen Y, Lin X, Wu Y, et al. Neoantimycin F, a streptomyces-derived natural product induces mitochondria-related apoptotic death in human non-small cell lung cancer cells. *Front Pharmacol* 2019;**10**:1042.
33. Zhou Y, Lin X, Williams SR, Liu L, Shen Y, Wang SP, et al. Directed accumulation of anticancer depsipeptides by characterization of neoantimycins biosynthetic pathway and an NADPH-dependent reductase. *ACS Chem Biol* 2018;**13**:2153−60.
34. Lehtio L, Chi NW, Krauss S. Tankyrases as drug targets. *FEBS J* 2013; **280**:3576−93.
35. Zamudio-Martinez E, Herrera-Campos AB, Munoz A, Rodriguez-Vargas JM, Oliver FJ. Tankyrases as modulators of pro-tumoral functions: molecular insights and therapeutic opportunities. *J Exp Clin Cancer Res* 2021;**40**:144.
36. Riccio AA, McCauley M, Langelier MF, Pascal JM. Tankyrase sterile alpha motif domain polymerization is required for its role in Wnt signaling. *Structure* 2016;**24**:1573−81.
37. Huang SM, Mishina YM, Liu S, Cheung A, Stegmeier F, Michaud GA, et al. Tankyrase inhibition stabilizes axin and antagonizes Wnt signalling. *Nature* 2009;**461**:614−20.
38. Chen B, Dodge ME, Tang W, Lu J, Ma Z, Fan CW, et al. Small molecule-mediated disruption of Wnt-dependent signaling in tissue regeneration and cancer. *Nat Chem Biol* 2009;**5**:100−7.
39. Shirai F, Mizutani A, Yashiroda Y, Tsumura T, Kano Y, Muramatsu Y, et al. Design and discovery of an orally efficacious spiroindolinone-based tankyrase inhibitor for the treatment of colon cancer. *J Med Chem* 2020;**63**:4183−204.
40. Waaler J, Machon O, Tumova L, Dinh H, Korinek V, Wilson SR, et al. A novel tankyrase inhibitor decreases canonical Wnt signaling in colon carcinoma cells and reduces tumor growth in conditional APC mutant mice. *Cancer Res* 2012;**72**:2822−32.
41. Stratford EW, Daffinrud J, Munthe E, Castro R, Waaler J, Krauss S, et al. The tankyrase-specific inhibitor JW74 affects cell cycle progression and induces apoptosis and differentiation in osteosarcoma cell lines. *Cancer Med* 2014;**3**:36−46.
42. Voronkov A, Holsworth DD, Waaler J, Wilson SR, Ekblad B, Perdreau-Dahl H, et al. Structural basis and SAR for G007-LK, a lead stage 1,2,4-triazole based specific tankyrase 1/2 inhibitor. *J Med Chem* 2013;**56**:3012−23.
43. Deng S, Zhou H, Xiong R, Lu Y, Yan D, Xing T, et al. Over-expression of genes and proteins of ubiquitin specific peptidases (USPs) and proteasome subunits (PSs) in breast cancer tissue observed by the methods of RFDD-PCR and proteomics. *Breast Cancer Res Treat* 2007;**104**:21−30.
44. Li J, Tan Q, Yan M, Liu L, Lin H, Zhao F, et al. miRNA-200c inhibits invasion and metastasis of human non-small cell lung cancer by directly targeting ubiquitin specific peptidase 25. *Mol Cancer* 2014;**13**:166.
45. Shibata N, Ohoka N, Tsuji G, Demizu Y, Miyawaza K, Ui-Tei K, et al. Deubiquitylase USP25 prevents degradation of BCR-ABL protein and ensures proliferation of Ph-positive leukemia cells. *Oncogene* 2020; **39**:3867−78.